PNAS RESEARCH ARTICLE | BIOPHYSICS AND COMPUTATIONAL BIOLOGY

Molten globule–like transition state of protein barnase measured with calorimetric force spectroscopy

Marc Rico-Pasto[a], Annamaria Zaltron[b], Sebastian J. Davis[c], Silvia Frutos[d], and Felix Ritort[a,1]

Edited by Dave Thirumalai, The University of Texas at Austin, Austin, TX; received July 5, 2021; accepted January 31, 2022 by Editorial Board Member Yale E. Goldman

Understanding how proteins fold into their native structure is a fundamental problem in biophysics, crucial for protein design. It has been hypothesized that the formation of a molten globule intermediate precedes folding to the native conformation of globular proteins; however, its thermodynamic properties are poorly known. We perform single-molecule pulling experiments of protein barnase in the range of 7 °C to 37 °C using a temperature-jump optical trap. We derive the folding free energy, entropy and enthalpy, and heat capacity change (ΔC_p = 1,050 ± 50 cal/mol·K) at low ionic strength conditions. From the measured unfolding and folding kinetic rates, we also determine the thermodynamic properties of the transition state, finding a significant change in ΔC_p (∼90%) between the unfolded and the transition states. In contrast, the major change in enthalpy (∼80%) occurs between the transition and native states. These results highlight a transition state of high energy and low configurational entropy structurally similar to the native state, in agreement with the molten globule hypothesis.

thermodynamics | protein | folding | transition state | molten globule

Significance

Understanding the molecular forces driving the unfolded polypeptide chain to self-assemble into a functional native structure remains an open question. However, identifying the states visited during protein folding (e.g., the transition state between the unfolded and native states) is tricky due to their transient nature. Here, we introduce calorimetric force spectroscopy in a temperature jump optical trap to determine the enthalpy, entropy, and heat capacity of the transition state of protein barnase. We find that the transition state has the properties of a dry molten globule, that is, high free energy and low configurational entropy, being structurally similar to the native state. This experimental single-molecule study characterizes the thermodynamic properties of the transition state in funneled energy landscapes.

Protein folding stands as one of the major open questions in biophysics. In the 1950–1960s decade, Anfinsen introduced the thermodynamic hypothesis claiming that proteins spontaneously fold to a free-energy minimum under appropriate conditions (1, 2). In 1969, Levinthal (3) noticed a polypeptide chain could not fold into the native state (hereafter denoted as N) by random search in configurational space. Protein folding is akin to finding a needle in a haystack and must be driven by molecular forces (4). In an effort to solve the paradox, Ptitsyn (5) proposed the molten globule hypothesis (MGH) where folding is similar to solid formation from a gas: A molten globule state must precede protein folding, similarly to the metastable liquid phase preceding solid formation during gas deposition. The dry molten globule is a necessary intermediate (6, 7) to form the N that is structurally similar to it but with most native bonds not yet formed. For years, scientists have searched for folding intermediates, the most natural solution to Levinthal's paradox. While these have been identified in large proteins, many small globular proteins fold in a two-states manner, raising the question whether such a molten globule intermediate does exist. Methods such as the phi-value analysis have shown that the transition state (hereafter referred to as TS) of two-state globular proteins is structurally similar to the N (8–10). The TS of two-state folders is a disguised molten globule of very short lifetime whose thermodynamic properties reflect those of the molten globule intermediate. In contrast to an intermediate state, defined as a local minimum in the free-energy landscape, the TS corresponds to a local maximum in the free-energy landscape.

A new direction of thought emerged in the late 1980s from Wolynes and coworkers (11, 12), who proposed the energy landscape hypothesis (ELH): Proteins fold in a funnel-like energy landscape by following different and productive folding trajectories. Albeit not excluded, intermediates are not obligatory folding steps. In both scenarios, MGH and ELH, the thermodynamics of the TS has generic and unique properties: On the one hand, a large energy barrier separates TS and N; on the other hand, there is a large configurational entropy loss upon forming the TS from the random coil or unfolded state (hereafter denoted as U). More recently, the alternative foldon hypothesis (FH) has gained considerable attention (13, 14), based on the accumulated evidence gathered from hydrogen exchange, NMR, and mass spectrometry studies. In the FH, proteins fold following a unique pathway by the cooperative and sequential formation of native structure domains (denoted as foldons). Folding amounts to the productive tinkering of amino acids and foldons rather than the diffusion of a polypeptide in a funnel-like energy landscape.

To evaluate the different hypotheses, computer simulations and experiments are employed (15, 16). For the latter, it is crucial to have tools for accurately measuring the thermodynamics and kinetics of folding. Besides bulk techniques (NMR, mass

Author contributions: F.R. designed research; M.R.-P. and S.J.D. performed research; S.F. contributed new reagents/analytic tools; M.R.-P. analyzed data; and M.R.-P., A.Z., and F.R. wrote the paper.

The authors declare no competing interest.

This article is a PNAS Direct Submission. D.T. is a guest editor invited by the Editorial Board.

[1]To whom correspondence may be addressed. Email: ritort@ub.edu.

This article contains supporting information online at https://www.pnas.org/lookup/suppl/doi:10.1073/pnas.2112382119/-/DCSupplemental.

Published March 10, 2022.

spectrometry, calorimetry, etc.), single-molecule fluorescence and force spectroscopy offer complementary insights on the protein folding problem. With these, individual proteins are manipulated and monitored with enough temporal resolution to detect short-lived intermediates (17–19), and measure transition path times along kinetic barriers (20). Key results are the demonstration that the ribosome promotes the efficient folding of the nascent polypeptide chain (21), and the role of protein mechanical properties on nuclear translocation (22). Single-molecule evidence of protein folding intermediates has been reported for RNAseH (23, 24), the coiled-coil leucine zipper (25, 26), and calmodulin (27). Recently, the molten globule of apomyoglobin has been shown to be highly deformable under force (28), and an off-pathway molten globule has been observed in apoflavodoxin (29). In other cases, proteins fold in a two-states manner without detectable intermediates [e.g., PrP protein (26)], and a molten globule of very short lifetime transiently forms along the folding pathway (30, 31).

Over the last decade, there has been much effort in determining the thermodynamic properties of intermediate states and TSs in globular proteins. How much do the enthalpy and entropy of the TS differ from the N? What is the heat capacity change (ΔC_p) between the TS and the N and U conformations? How do the TS properties change by varying the external conditions (e.g., temperature, ionic strength, and pH)? Answering these questions is essential to understand the features of the different hypotheses (e.g., the liquid-like properties of the molten globule in the MGH or the funnel's shape in the ELH), and the nature of the folding process itself.

Upon heating, proteins melt at a characteristic temperature T_m at which the heat capacity at constant pressure, C_p, shows a peak (32, 33). The heat capacity change upon folding, ΔC_p, can be used to determine temperature-dependent enthalpy and entropy differences (34, 35). Moreover, ΔC_p is directly related to the change in the number of degrees of freedom (dof), Δn, across the transition, $\Delta C_p = \Delta n \cdot k_B/2$. Therefore, ΔC_p quantifies the configurational entropy loss, the main contribution to the folding entropic barrier.

Laser optical tweezers (36) are suitable for calorimetric measurements; however, most studies have been carried out at ambient temperature $T_{\text{room}} = 298$ K (37–39), due to the difficulty of controlling temperature (40, 41). For many years, this limitation has challenged direct enthalpy and entropy measurements over a wide range of temperatures, rendering ΔC_p inaccessible to single-molecule assays. We have recently built a temperature-jump optical trap suitable for single-molecule force spectroscopy above and below T_{room}, thus providing a calorimetric force spectroscopy (CFS) tool for molecular thermodynamics (42, 43). Here, we investigate the folding thermodynamics and kinetics of protein barnase, a paradigmatic model in protein folding studies (Fig. 1*A*). Barnase is a 110-aa bacterial ribonuclease globular protein secreted by *Bacillus amyloliquefaciens*, which, in physiological conditions, degrades RNA in the absence of its protein inhibitor barstar (45). The high solubility and stability of barnase makes it an excellent model to investigate the folding kinetics of globular proteins, by combining phenomenological approaches (e.g., the phi-value analysis) with protein engineering and site-directed mutagenesis methods (8). Barnase reversibly folds in a two-states manner between the unfolded and native conformations. It has been suggested that barnase folds via a short-lived intermediate (31, 46, 47) and two TSs (48). However, pulling experiments at room temperature could not find evidence of intermediates down to milliseconds (49). Here, we pull barnase in the range 7 °C to 37 °C and derive thermodynamic quantities by combining fluctuation theorems for free-energy prediction and kinetics. We determine the temperature-dependent folding free energy (ΔG), entropy (ΔS), and enthalpy (ΔH), to derive ΔC_p (∼1,000 cal/mol·K). Our results are consistent with calorimetry studies under similar ionic strength and pH conditions.

We also determine the entropy, enthalpy, and ΔC_p of the TS, finding that it is structurally similar to N. Upon folding, most of the enthalpy and entropy change occurs between N and TS, where roughly 80% of the native bonds are formed (from molten to native). In contrast, most of the folding ΔC_p occurs between U and TS, with ∼90% of configurational entropy loss. The collapse from TS to N mostly contributes to the enthalpy and entropy of folding, but residually to ΔC_p. Our results demonstrate that the TS has the properties of a dry molten globule: a large entropy and enthalpy relative to the N and a low configurational entropy. Albeit structurally similar to the N, the molten globule is a high-energy state with most bonds not formed.

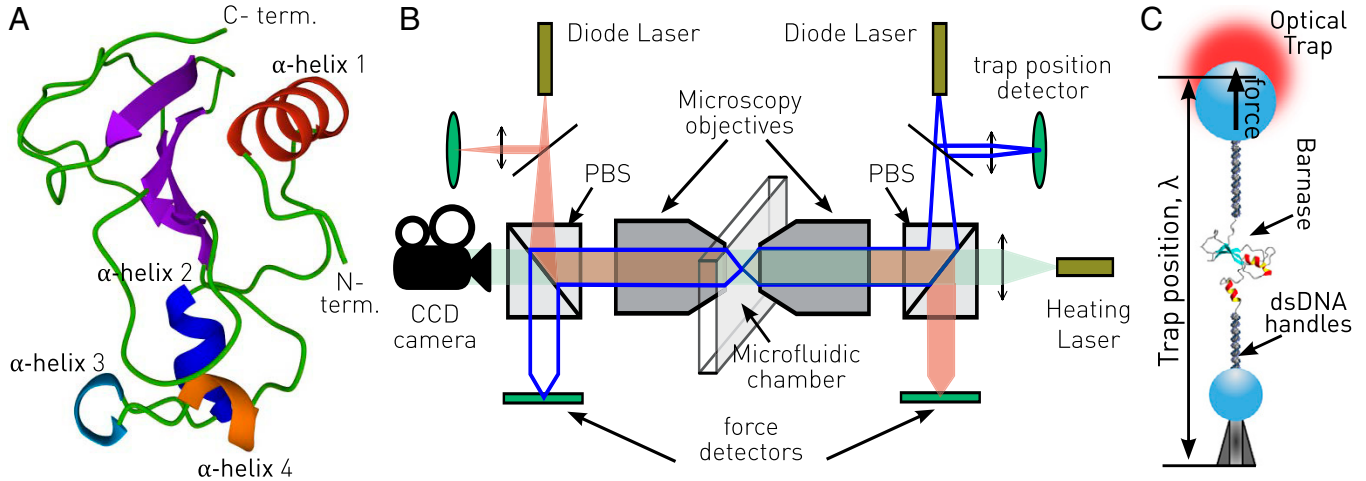

Fig. 1. CFS of protein barnase. (*A*) Three-dimensional view of native barnase obtained with X-ray diffraction with 1.50-Å resolution (44). Four external α-helices (helix 1: Phe7-Tyr17 [red]; helix 2: Lys27-Leu33 [blue]; helix 3: Ala37-Lys39 [cyan]; helix 4: Leu42-Val45 [orange]) contain a total of 25 amino acids surrounding four β-strands (purple) located in the protein core. (*B*) Schematics of the temperature-jump optical trap setup. The diode lasers (red and blue) form a single optical trap, while the collimated heating laser (green) passes through the microfluidic chamber. CCD, charge-coupled device; PBS, polarizing beam splitter. (*C*) Illustration of the molecular construct and experimental setup: barnase is flanked by two identical 500-bp dsDNA handles and tethered between two beads. One bead is captured in the optical trap while the other one is kept fixed by air suction on the tip of a glass micropipette.

Results

Force–Distance Curves. Barnase was inserted in a molecular construct that was tethered between two beads and mechanically pulled with a temperature-jump optical trap (Fig. 1 *B* and *C* and *Materials and Methods*). Force–distance curves (FDCs) were measured by repeatedly pulling barnase between minimum and maximum force values at different temperatures. Fig. 2*A* shows FDCs of five selected pulling cycles (unfolding and refolding) for the six investigated temperatures (7 °C, 14 °C, 18 °C, 25 °C, 32 °C, and 37 °C). It is apparent that the lower the temperature, the higher the unfolding force and the FDC hysteresis. In Fig. 2*B*, we show a single pulling cycle at 25 °C. During stretching (red curve), barnase unfolding is observed as a sudden force rip ($\Delta f \approx$ 2 pN) in the FDC at forces 15 pN to 30 pN. Upon force release (blue curve), a folding transition is detected as a small force jump ($\sim$0.5 pN) at forces $\lesssim$5 pN. The encircled zoomed Fig. 2 *B*, *Left Inset* shows the two force branches where barnase is folded (N branch, black dashed line) and unfolded (U branch, gray solid line). N and U branches describe the elastic response of the molecular construct where barnase is in N and U, respectively. The relative trap position (λ) in the two branches contains the trap bead displacement plus the handles extension and the molecular extension. The difference between the two branches at a given force, $\Delta\lambda$ (Fig. 2 *B*, *Right Inset*), is the difference of molecular extensions between the polypeptide chain and the projection on the force axis of the dipole formed by the N and C termini of barnase.

Folding Free Energy, Entropy, and Enthalpy. Here we describe how to extract the temperature-dependent folding free energy of barnase at zero force, $\Delta G_0(T)$, from the measured free-energy difference $\Delta G(T)$. $\Delta G_0 = G_{\rm U} - G_{\rm N}$ equals the (positive) free-energy difference between the native conformation (N) and the random coil state (unfolded, U). The nomenclature for free-energy differences employed throughout the paper is the standard one in single-molecule and calorimetric bulk studies. ΔG_0 can be measured in bulk assays at zero force, whereas CFS experiments measure free-energy differences at a given force, $\Delta G(f)$. To derive ΔG_0 from $\Delta G(f)$, it is necessary to subtract contributions coming from the experimental setup, such as the displacement of the bead from the center of the optical trap and the stretching of the handles and the polypeptide chain (50). The procedure is illustrated in Fig. 2*C* where the different stretching contributions correspond to free-energy differences measured over three distinct steps ($1 \to 2; 2 \to 3; 3 \to 4$). $\Delta G_0(T)$ can be derived (*Materials and Methods*) from the measured $\Delta\lambda(f, T)$ and the coexistence force in equilibrium, $f_c(T)$ (defined by $G_{\rm N} = G_{\rm U}$ or $\Delta G(f_c(T)) = 0$),

$$\Delta G_0(T) = \int_0^{f_c(T)} \Delta\lambda(f, T)\, df. \qquad [1]$$

From Eq. **1**, we derive the folding entropy and enthalpy, $\Delta S_0 = -\partial\Delta G_0/\partial T$ and $\Delta H_0 = \Delta G_0 - T\Delta S_0$. For the entropy, we find

$$\Delta S_0(T) = -\frac{\partial f_c(T)}{\partial T}\Delta\lambda(f_c(T)) - \int_0^{f_c(T)} \frac{\partial\Delta\lambda(f', T)}{\partial T} df'. \qquad [2]$$

This is analogous to the Clausius–Clapeyron equation for first-order phase transitions, where f and λ are the equivalent of pressure and volume (42). The second term in Eq. **2** is the entropic contribution to stretch and orient the protein dipole from zero force to f_c. Eqs. **1** and **2** require measuring $\Delta\lambda(f, T)$ over the full integration range, [0, $f_c(T)$], and $f_c(T)$. While $\Delta\lambda$ is directly obtained from the FDCs (Fig. 2 *B*, *Right Inset*), the value of $f_c(T)$ is unknown due to the strongly irreversible FDCs. The $f_c(T)$ might be extracted from equilibrium hopping experiments; however, this is not possible in barnase, due to the exceedingly long hooping times (25, 26). Here we derive $f_c(T)$ by measuring $\Delta G_0(T)$ using the fluctuation theorem (*Measurement of Folding Free Energy*) and using Eq. **1**.

Elastic Response of the Polypeptide Chain. The temperature-dependent elastic properties of the polypeptide chain were determined using the molecular extension $x_{\rm p}(f, T)$ obtained from $\Delta\lambda(f, T)$ (Fig. 2*B*) and the dipole contribution $x_{\rm d}(f, T)$ from $x_{\rm p} = \Delta\lambda + x_{\rm d}$. In Fig. 3*A*, we show f versus $\Delta\lambda$ measured at three selected temperatures (7 °C, 25 °C, and 37 °C). To extract

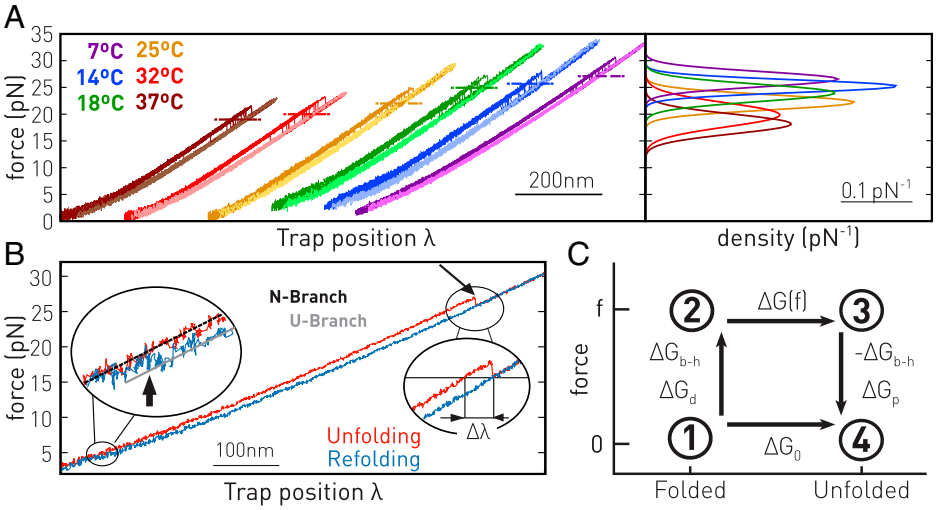

Fig. 2. Pulling experiments of protein barnase. (*A*) (*Left*) Unfolding (dark) and folding (light) FDCs at different temperatures, 7 °C (purple), 14 °C (blue), 18 °C (green), 25 °C (yellow), 32 °C (red), and 37 °C (brown). FDCs at each temperature have been shifted along the *x* axis for clarity. Horizontal dashed lines denote the most probable unfolding force at each temperature. (*Right*) Unfolding force distributions for all the studied temperatures. For sake of clarity, we show Gaussian fits to histograms. For higher temperatures, less force is required to unzip the protein. (*B*) Unfolding (red) and refolding (blue) trajectories at 25 °C. (*Left Inset*) Zoomed refolding event (arrow) from the U branch (gray solid line) to the N branch (black dashed line). (*Right Inset*) Zoomed unfolding event (arrow) highlighting $\Delta\lambda$. (*C*) Scheme of the different thermodynamic steps to measure ΔG_0. Stretching of the folded protein ($1 \to 2$), unfolding at a given force ($2 \to 3$), releasing of the unfolded protein ($3 \to 4$), and unfolding at zero force ($1 \to 4$).

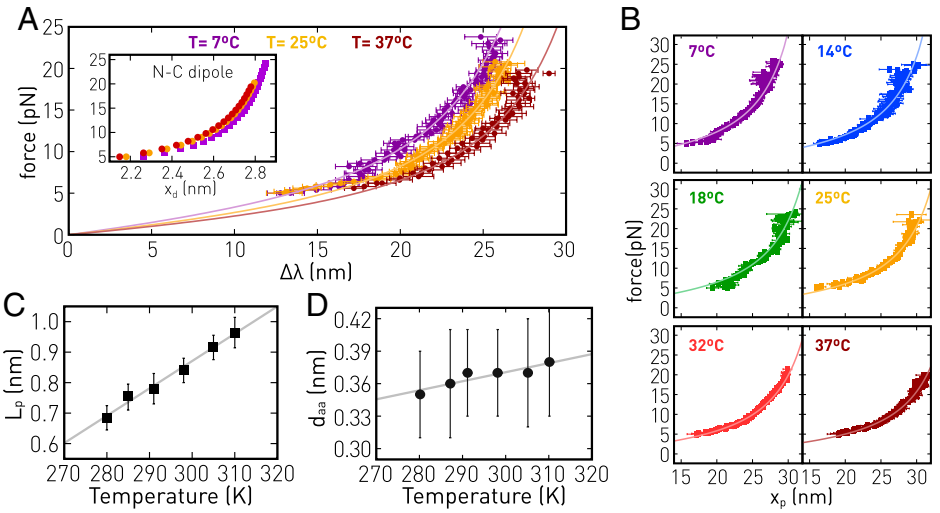

Fig. 3. Elastic response of the polypeptide chain. (*A*) Force versus difference in trap position ($\Delta\lambda$) at three temperatures: 7 °C (purple), 25 °C (yellow), and 37 °C (brown). (*Inset*) Elastic response of the folded protein modeled as a dipole of 3 nm with the FJC model. (*B*) Fits of the measured force versus polypeptide chain extension (x_p) to the WLC model (solid lines). (*C*) Persistence length (L_p) and (*D*) amino acid distance (d_{aa}) of the polypeptide chain calculated from the fits in *B*. Solid lines are linear fits to the experimental points.

$x_p(f, T)$ from Eq. **15**, we modeled the dipole extension $x_d(f, T)$ with the freely jointed chain elastic model (Fig. 3 *A*, *Inset*), assuming that the distance between the N and C termini for the folded barnase (the dipole length taken equal to 3 nm) is constant with temperature. By comparing Fig. 3*A* and Fig. 3 *A*, *Inset*, we observe that $x_d(f, T) \ll \Delta\lambda(f, T)$, as expected, since the dipole length is much shorter than the polypeptide extension. Therefore, $x_p(f, T)$ increases with T at a given f, making the polypeptide chain stiffer with temperature. The $x_p(f, T)$ is well described by the inextensible worm-like chain (WLC) model and its interpolation equation (51),

$$f = \frac{k_B T}{4L_p}\left(\left(1 - \frac{x_p(T)}{N_{aa}\cdot d_{aa}}\right)^{-2} + 4\cdot\frac{x_p(T)}{N_{aa}\cdot d_{aa}} - 1\right), \quad [3]$$

where L_p is the persistence length, N_{aa} is the number of residues (110 for barnase), and d_{aa} is the distance between consecutive amino acids. The data relative to each investigated temperature were fit to Eq. **3**, as shown in Fig. 3*B*, with L_p and d_{aa} as free parameters. As reported in Fig. 3*C*, L_p shows a strong T dependence, which is well approximated by a linear function of slope 0.011 ± 0.001 nm/K. Similar results are obtained if we fit the data with a perturbative expansion of the WLC model (52) instead of Eq. **3**. Moreover, d_{aa} presents a weak T-linear dependence of slope 0.0008 ± 0.0002 nm/K (Fig. 3*D*), which is one order of magnitude smaller than for L_p. Therefore, d_{aa} can be taken as constant, ∼0.37 nm. Both fitting parameters at room temperature (298 K) agree with previous results (47, 49).

Measurement of Folding Free Energy. To derive ΔG_0, we use the thermodynamic relation illustrated in Fig. 2*C*, that relates ΔG_0 with the elastic contributions of the polypeptide chain ΔG_p, the dipole term ΔG_d, and $\Delta G(f)$ (Eq. **12** in *Materials and Methods*),

$$\Delta G_0 = \Delta G_d(0 \to f) + \Delta G(f) - \Delta G_p(0 \to f). \quad [4]$$

From the results of the previous section, we can readily determine ΔG_p and ΔG_d; however, how to measure $\Delta G(f)$ remains unanswered. In optical tweezers experiments, the relative trap position λ is the control parameter, rather than the force which fluctuates depending on the molecular state. A thermodynamic relation similar to Eq. **4** holds by a Legendre transforming $f \to \lambda$ to the λ-ensemble (*SI Appendix*, section S1). ΔG_0 is determined by measuring the free-energy difference, ΔG_λ, between minimum and maximum trap positions where barnase is folded (λ_{min}) and unfolded (λ_{max}),

$$\Delta G_0 = \Delta G_\lambda - W_\lambda^{elas}, \quad [5]$$

where W_λ^{elas} stands for the elastic contributions of the setup (bead, handles, polypeptide chain, and protein dipole) that must be subtracted to ΔG_λ (*SI Appendix*, section S1).

We used the work fluctuation theorem (work-FT) (53, 54) to determine ΔG_λ from irreversible work (W) measurements by integrating the FDC between the two selected trap positions, $W = \int_{\lambda_{min}}^{\lambda_{max}} f d\lambda$ (Fig. 4*A*). Let $P_U(W)$ and $P_F(W)$ denote the unfolding and folding work distributions measured over many pulling cycles. The work-FT is given by

$$\frac{P_U(W)}{P_F(-W)} = \exp\left(\frac{W - \Delta G_\lambda}{k_B T}\right), \quad [6]$$

where ΔG_λ equals the reversible work. The minus work sign in $P_F(-W)$ in the left-hand-side of Eq. **6** is a consequence of the fact that $W < 0$ in the folding process. A corollary of Eq. **6** is the Jarzynski equality, $\Delta G_\lambda = -k_B T \log\langle\exp(-W/k_B T)\rangle$, where $\langle(\ldots)\rangle$ is the average over many (infinite) realizations. In practice, the number of pulls is finite, and the Jarzynski equality is strongly biased (55). From Eq. **6**, work distributions cross at $W = \Delta G_\lambda$; that is, $P_U(\Delta G_\lambda) = P_F(-\Delta G_\lambda)$. However, the crossing point is not observed, due to the hysteresis of the FDCs, quantified by the area enclosed between the unfolding and folding FDC (Fig. 4*A*). The dissipated work is in the range 50 $k_B T$ to 100$k_B T$, and much larger than the value of ΔG_0 (see below). In the absence of crossing, one can use the matching method (53), that gives reasonable free-energy estimates and is simpler than other mathematical approaches (55, 56). In this method, the value of ΔG_λ is determined by matching the functions $P_U(W)$ and $P_F(-W)\exp((W - \Delta G_\lambda)/k_B T)$. In practice, the leftmost (rightmost) tails of $P_U(W)$ ($P_F(-W)$) are fitted to the generic form, $\sim\exp\left(-|W - W_{max}|^\delta/\Omega\right)$, to extract the values of δ, Ω, W_{max} (55). In Fig. 4 *B*, *Top*, we show $P_U(W)$, $P_F(-W)$ at 25 °C and the fitted tails. Rightmost (P_F)

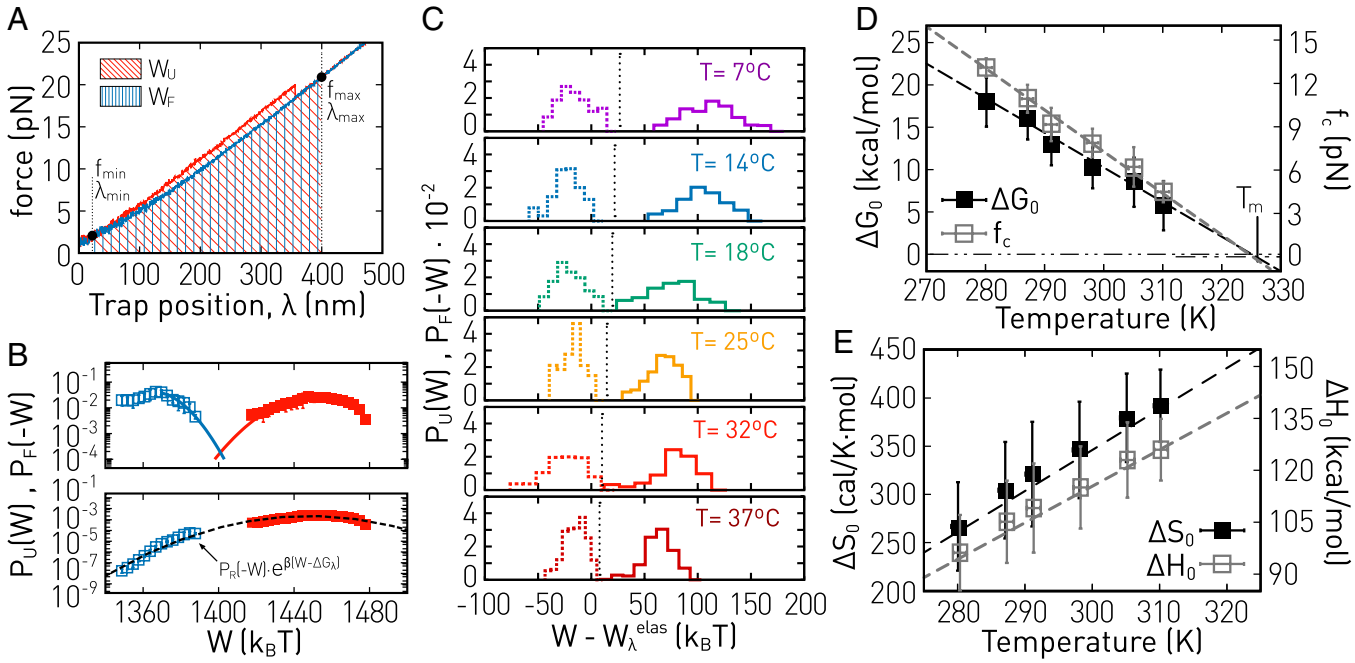

Fig. 4. Folding thermodynamics of barnase. (*A*) Work measurements from unfolding (red) and folding (blue) FDC. The unfolding and folding work W is the area below the FDC limited by λ_{min} and λ_{max} (red and blue areas). (*B*) (*Top*) Unfolding (red full squares) and folding (blue empty squares) work distributions at 25 °C. (*Bottom*) $P_U(W)$ and $P_F(-W)$ times $\exp((W-\Delta G_\lambda)/k_BT)$. The black dashed line is a Gaussian fit to determine ΔG_λ. (*C*) Unfolding (solid line) and folding (dashed lines) work distributions at different temperatures (with the elastic contribution W_λ^{elas} being subtracted from the total work). The dotted vertical line indicates ΔG_0 for each temperature. (*D*) Solid squares are the estimated ΔG_0 versus T, and black dashed line is a fit to $\Delta G_0(T) = \Delta H_0^m - T\Delta S_0^m$. Empty squares are the estimated coexistence force, and dashed gray line is a linear fit to f_c. (*E*) Solid and empty squares are the entropy and enthalpy differences at zero force. Dashed lines are fits to Eqs. **7a** and **7b**, respectively.

and leftmost (P_U) tails are well fitted with $\delta \approx 1.9$, indicating Gaussian-like tails ($\delta = 2$). Therefore, we simultaneously fitted $P_U(W)$ and $P_F(-W)\exp((W-\Delta G_\lambda)/k_BT)$ to a single Gaussian distribution (black dashed line in Fig. 4 *B*, *Bottom*) to find the best matching the value of ΔG_λ. The fact that the generic and Gaussian distributions are nearly the same and a single Gaussian distribution (dashed line in Fig. 4 *B*, *Bottom*) simultaneously fits $P_U(W)$ and $P_F(-W)\exp(W-\Delta G_\lambda)/k_BT)$ demonstrates that $\delta \approx 2$ is an excellent approximation to $P_U(W)$ and $P_F(-W)$ tails around $W = \Delta G_\lambda$ (*SI Appendix*, Fig. S1).

To determine ΔG_0 from ΔG_λ in Eq. **5**, we subtract the elastic contributions as follows: The bead contribution was calculated by modeling the optical trap with Hooke's law, that is, a constant optical trap's stiffness equal to 0.07 pN/nm throughout the explored force range (50, 57); the DNA handles term was calculated by integrating the WLC model with the temperature-dependent elastic parameters from ref. 58; ΔG_p and ΔG_d contributions were calculated using the elastic parameters from *Elastic Response of the Polypeptide Chain*. In Fig. 4*C*, we show the $P_U(W)$ and $P_F(-W)$ at different temperatures. Distributions are plotted versus $W - W_\lambda^{elas}$ instead of W, to directly determine ΔG_0 with the matching method (Fig. 4*C*, dotted vertical lines). The values of $\Delta G_0(T)$ present a clear temperature dependence (Fig. 4*D*, filled black squares) as expected from the relation $\Delta G_0 = \Delta H_0 - -T\Delta S_0$.

Derivation of entropy and enthalpy. From Eq. **1** and the measured values of $\Delta G_0(T)$ and $\Delta\lambda(f,T)$ (*Elastic Response of the Polypeptide Chain*), we derive $f_c(T)$ in the range 7 °C to 37 °C (gray empty squares in Fig. 4*D*). The $f_c(T)$ decreases linearly with T, thus defining an $f-T$ phase diagram separating the N and U. We note that the linear trend observed in Fig. 4*D* does not agree with predictions by lattice models (59–61) for the critical force at which the fraction of native contacts equals 0.5 (*SI Appendix*, Figs. S3 and S4). The line $f_c(T)$ crosses the T axis at $T_m \simeq 50$ °C, in agreement with bulk experiments (see below). Finally, from Eq. **2** and $f_c(T)$, we derived $\Delta S_0(T)$ (black solid squares in Fig. 4*E*). It changes by roughly 22% in the whole temperature range, indicating a finite ΔC_p. Notice that the numerical T derivative of $\Delta G_0(T)$ is roughly constant (Fig. 4*D*), which confirms Eq. **2** as the most reliable way to estimate $\Delta S_0(T)$. Folding enthalpies, $\Delta H_0 = \Delta G_0 + T\Delta S_0$, are shown in Fig. 4*E* (empty squares).

Heat capacity change. Bulk assays have shown that barnase has a finite ΔC_p. The marked temperature dependence in ΔS_0 and ΔH_0 (Fig. 4*E*) allows us to extract ΔC_p across the melting transition. To do so, we expand ΔH_0 and ΔS_0 around the melting temperature T_m,

$$\Delta S_0(T) = \Delta S_0^m + \Delta C_p \cdot \log\left(\frac{T}{T_m}\right) \qquad [7a]$$

$$\Delta H_0(T) = \Delta H_0^m + \Delta C_p \cdot (T - T_m), \qquad [7b]$$

where ΔS_0^m and $\Delta H_0^m = T_m\Delta S_0^m$ are the entropy and enthalpy at T_m, and ΔC_p is the heat capacity change between N and U. $\Delta S_0(T)$ and $\Delta H_0(T)$ were fitted to Eqs. **7a** and **7b** (dashed lines in Fig. 4*E*) with ΔC_p, ΔH_0^m, ΔS_0^m, and T_m fitting parameters. We obtain $\Delta C_p = 1,030 \pm 43$ cal/mol·K, $\Delta S_0^m = 431 \pm 10$ cal/mol·K, and $\Delta H_0^m = 140 \pm 6$ kcal/mol.

Kinetics. The results derived from the work-FT are confronted with those derived from the temperature-dependent unfolding and folding kinetic rates using the same experimental FDCs. Fig. 5*A* shows the unfolding and folding force distributions ($\rho_\rightarrow(f)$, $\rho_\leftarrow(f)$) at three selected temperatures (7 °C, 25 °C, and 37 °C). We extract the unfolding and folding kinetic rates, $k_\rightarrow(f)$ and $k_\leftarrow(f)$, from the corresponding survival probabilities. If f is ramped at constant loading rate $r = |df/dt|$, the following relations hold:

$$\frac{dP_N(f)}{df} = -\frac{k_{\rightarrow}(f)}{r} P_N(f) \;\Rightarrow\; k_{\rightarrow}(f) = r\,\frac{\rho_{\rightarrow}(f)}{P_N(f)} \qquad \textbf{[8a]}$$

$$\frac{dP_U(f)}{df} = \frac{k_{\leftarrow}(f)}{r} P_U(f) \;\Rightarrow\; k_{\leftarrow}(f) = r\,\frac{\rho_{\leftarrow}(f)}{P_U(f)}, \qquad \textbf{[8b]}$$

with $P_N(f) = 1 - \int_0^f \rho_{\rightarrow}(f)\,df$ and $P_U(f) = 1 - \int_f^{\infty} \rho_{\leftarrow}(f)\,df$ being the survival probabilities of N and U, respectively. Our measurements of $k_{\rightarrow}(f)$ and $k_{\leftarrow}(f)$ are shown in Fig. 5*B* in a log-normal scale, for all the studied temperatures. The force dependence of the kinetic rates is described by

$$k_{\rightarrow}(f) = k_a \exp\left(-\frac{\Delta G^{\ddagger}(f)}{k_B T}\right) \qquad \textbf{[9a]}$$

$$k_{\leftarrow}(f) = k_a \exp\left(-\frac{\Delta G^{*}(f)}{k_B T}\right), \qquad \textbf{[9b]}$$

with k_a as the attempt rate and $\Delta G^{\ddagger}(f)$ ($\Delta G^{*}(f)$) as the force-dependent kinetic barrier relative to N (U). An illustrative free-energy landscape is shown in Fig. 5*C*, highlighting $\Delta G(f)$, $\Delta G^{\ddagger}(f)$, and $\Delta G^{*}(f)$. Notice the hysteresis between unfolding and folding (a minimum of a ∼10-pN gap is observed between the measured unfolding and folding rates; Fig. 5*B*). This fact precludes us from determining the coexistence force and the folding free energy at zero force using Eq. **1**. To circumvent this problem, we have determined the force dependence of the unfolding and folding kinetic rates beyond the Bell–Evans model, where distances of N and U to the TS are taken as force independent (62, 63). To do so, we have used the detailed balance condition,

$$\frac{k_{\leftarrow}(f)}{k_{\rightarrow}(f)} = \exp\left(\frac{\Delta G(f)}{k_B T}\right), \qquad \textbf{[10]}$$

that relates the unfolding/folding kinetic rates with the energy difference between N and U at force *f*, $\Delta G(f)$ (compare Eq. **4**). For a given trial value of ΔG_0, the energy $\Delta G(f)$ is calculated using Eq. **10** with the elastic contributions determined in *Elastic Response of the Polypeptide Chain*. Then we used Eq. **10** to reconstruct the unfolding (folding) kinetic rates in the region of forces where folding (unfolding) transition events are observed in the pulling experiments. To estimate the quality of the continuity of the rates between the two force regimes, we have fitted the unfolding kinetic rates (measured and reconstructed) to a single quadratic function in the log-normal plot (dashed lines in Fig. 5*B*). From these fits and Eq. **10**, we inferred the folding kinetic rates (solid lines in Fig. 5*B*). This procedure has been repeated by varying ΔG_0 in the range of 2 kcal/mol to 20 kcal/mol in steps of 0.2 kcal/mol. To determine the $\Delta G_0(T)$ that best fits the data, we have minimized the χ^2 between the predicted force-dependent kinetic rates and the experimental and reconstructed rates (*SI Appendix*, Fig. S2). The curvature of the reconstructed log $k_{\rightleftarrows}$ vs. force plots at low forces (Fig. 5*B*) has been also observed for the ligand binding rates to filamin protein (64). The derived values for $\Delta G_0(T)$ are shown as black circles in Fig. 5 *D*, *Top*. In addition, using the extrapolated kinetic rates (solid and dashed lines in Fig. 5*B*), we determined the coexistence force f_c as the force value at which $k_{\rightarrow} = k_{\leftarrow}$ (empty gray circles in Fig. 5 *D*, *Top*).

From $\Delta\lambda(f, T)$, derived in *Elastic Response of the Polypeptide Chain*, and the values of $f_c(T)$ and $\Delta G_0(T)$ obtained from the kinetics analysis, we used Eq. **2** to calculate $\Delta S_0(T)$ and $\Delta H_0(T)$ (Fig. 5 *D*, *Bottom*, black circles and empty gray circles, respectively). These values agree with those obtained independently from the work-FT analysis (*SI Appendix*, Fig. S3). Fitting $\Delta S_0(T)$ and $\Delta H_0(T)$ to Eqs. **7a** and **7b** gives $\Delta C_p = 1,100 \pm 60$ cal/mol·K, $\Delta S_0^m = 437 \pm 8$ cal/mol·K, and $\Delta H_0^m = 141 \pm 3$ kcal/mol.

Furthermore, we determined the TS enthalpy and entropy differences, $\Delta S^{\ddagger}$, $\Delta H^{\ddagger}$, ΔS^{*}, and ΔH^{*}, relative to states N and U (Fig. 5*C*). To this aim, we rewrite the kinetic rates in Eqs. **9a** and **9b** at zero force, $k_{\leftarrow}^0$, $k_{\rightarrow}^0$, in terms of the TS entropies and enthalpies,

$$k_{\rightarrow}^0(T) = k_a \exp\left(\frac{\Delta S^{\ddagger}}{k_B}\right) \exp\left(-\frac{\Delta H^{\ddagger}}{k_B T}\right) \qquad \textbf{[11a]}$$

$$k_{\leftarrow}^0(T) = k_a \exp\left(\frac{\Delta S^{*}}{k_B}\right) \exp\left(-\frac{\Delta H^{*}}{k_B T}\right). \qquad \textbf{[11b]}$$

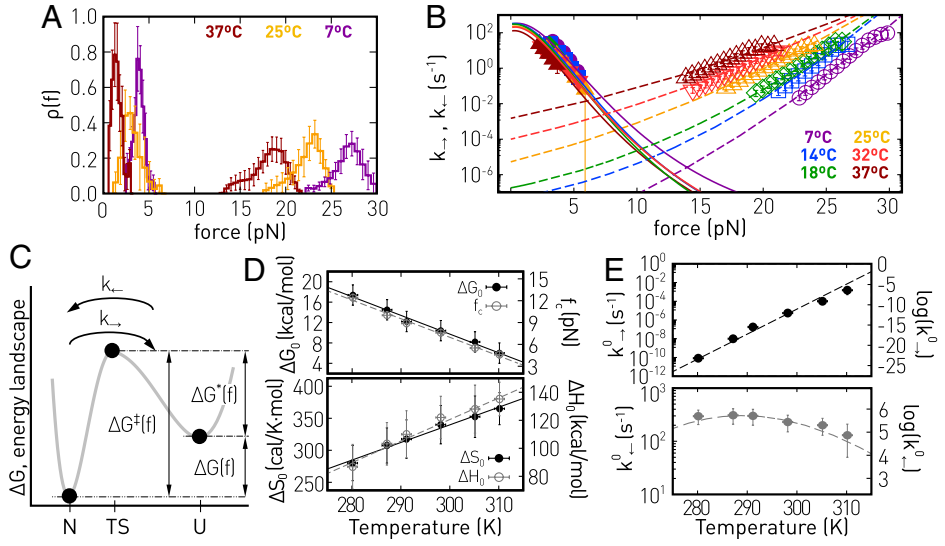

Fig. 5. Folding kinetics of barnase. (*A*) Unfolding (right) and refolding (left) force distributions at 7 °C (purple), 25 °C (yellow), and 37 °C (dark brown). (*B*) Force-dependent unfolding (empty symbols) and folding (solid symbols) kinetic rates for all temperatures, 7 °C (purple), 14 °C (blue), 18 °C (green), 25 °C (yellow), 32 °C (red), and 37 °C (brown). The solid (refolding) and dashed (unfolding) lines are fits to the Bell–Evans model. (*C*) Schematics of the folding free-energy landscape in the Bell–Evans model. (*D*) Folding free energy and coexistence force (*Top*) and entropy and enthalpy (*Bottom*) as a function of temperature. Dashed lines are fits to Eqs. **7a** and **7b**. (*E*) Unfolding (*Top*) and refolding (*Bottom*) kinetic rates at zero force versus $1/T$. Dashed lines are simultaneous fits to Eqs. **11a** and **11b**.

Table 1. Thermodynamic properties of barnase at three selected temperatures

T	ΔG_0	ΔH_0	ΔS_0	$\Delta G^{\ddagger}$	$\Delta H^{\ddagger}$	$\Delta S^{\ddagger}$	ΔG^{*}	ΔH^{*}	ΔS^{*}
7	17 ± 3	94 ± 11	273 ± 40	12 ± 4	101 ± 2	318 ± 14	-6 ± 4	6 ± 3	45 ± 15
14	15 ± 2	104 ± 12	310 ± 40	11 ± 4	103 ± 2	324 ± 14	-4 ± 3	0 ± 2	14 ± 11
18	13 ± 2	108 ± 13	327 ± 43	9 ± 4	104 ± 2	326 ± 14	-3 ± 3	-3 ± 2	-2 ± 10
25	10 ± 2	116 ± 12	353 ± 38	8 ± 5	105 ± 2	328 ± 15	-3 ± 3	-10 ± 2	-25 ± 11
32	8 ± 2	122 ± 12	372 ± 39	6 ± 4	106 ± 2	329 ± 13	-3 ± 3	-16 ± 2	-42 ± 11
37	6 ± 2	126 ± 10	387 ± 29	4 ± 3	108 ± 2	332 ± 12	-2 ± 3	-19 ± 2	-56 ± 10
50	0	140 ± 2	434 ± 10	2 ± 2	111 ± 2	337 ± 4	2 ± 3	-30 ± 2	-100 ± 8

T in degrees Celsius; ΔG and ΔH in kilocalories per mole; and ΔS in calories per mole kelvin. Thermodynamic potentials differences: 0, N–U; ‡, N–TS; and *, U–TS. Note that $\Delta_{\text{N-U}} = \Delta_{\text{N-TS}} - \Delta_{\text{U-TS}}$ or $\Delta_0 = \Delta^{\ddagger} - \Delta^{*}$ in our notation.

We performed a simultaneous fit of $k^0_{\rightarrow}$ and $k^0_{\leftarrow}$ to Eqs. **11a** and **11b** to derive the values of $\Delta S^{\ddagger}$, ΔS^{*},$\Delta H^{\ddagger}$, and ΔH^{*}. Interestingly, we found that $k^0_{\rightarrow}$ is strongly T dependent, while $k^0_{\leftarrow}$ depends weakly on T, hinting at an entropy-driven folding process. The four-parameters fit was done by imposing two constraints: $\Delta S^{*} = \Delta S^{\ddagger} - \Delta S_0$ and $\Delta H^{*} = \Delta H^{\ddagger} - \Delta H_0$. For the fits to Eqs. **11a** and **11b**, the values of $\Delta S_0(T)$ and $\Delta H_0(T)$ have been taken as the mean values obtained from the FT (Fig. 4*E*) and kinetics (Fig. 5 *D*, *Bottom*). Moreover, we used the attempt rate previously obtained on the same molecular system in similar experimental conditions (49), $k_a \approx 150\,\text{s}^{-1}$. Fits are shown as dashed lines in Fig. 5*E*. TS entropies and enthalpies are shown in Fig. 6*A* and in Table 1 at all studied temperatures and at the average T_m (50 °C). Fitting them to Eqs. **7a** and **7b** permits us to extract the heat capacity change between N and TS ($\Delta C_p^{\text{N-TS}}$) and between TS and U ($\Delta C_p^{\text{TS-U}}$). We obtain $\Delta C_p^{\text{N-TS}} \sim$150 cal/mol·K and $\Delta C_p^{\text{TS-U}} \sim$900 cal/mol·K, which gives the folding $\Delta C_p \sim$1,050 cal/mol·K.

The Folding Funnel. Fig. 6*A* and Table 1 summarize our main results: The energy differences between states N and U (ΔG_0, ΔH_0, and ΔS_0); the barrier energies to unfold, N-TS ($\Delta G^{\ddagger}$, $\Delta H^{\ddagger}$ and $\Delta S^{\ddagger}$); and the barrier energies to fold, U-TS (ΔG^{*}, ΔH^{*}, and ΔS^{*}). The energy parameters of the free-energy landscape of barnase (Fig. 5*C*) are illustrated in Fig. 6*B*. Results show that barrier entropies, enthalpies, and free energies to fold (U $\rightarrow$ TS) are one order of magnitude smaller than the corresponding barriers to unfold (N $\rightarrow$ TS): $|\Delta S^{*}| \ll |\Delta S^{\ddagger}|$, $|\Delta H^{*}| \ll |\Delta H^{\ddagger}|$, and $|\Delta G^{*}| \ll |\Delta G^{\ddagger}|$. This difference suggests a folding process in two steps (Fig. 6*C*). In the first step, the unfolded protein reaches a TS with a few H bonds (∼20%) formed relative to U. In the second step, the protein collapses into N by forming the rest of the native bonds (∼80%). These bond percentages are estimated from the different enthalpy values for the TS relative to N and U ($\Delta H^{\ddagger} \sim$109 kcal/mol and $\Delta H^{*} \sim$-30 kcal/mol at T_m).

A remarkable difference is found in ΔC_p between TS and N or U (Fig. 6*A*). The main contribution to the total $\Delta C_p = 1,065 \pm 50$ cal/mol·K comes from TS and U ($\Delta C_p^{\text{TS-U}} = 905 \pm 20$ cal/mol·K), which is ∼9 times larger than between N and TS ($\Delta C_p^{\text{N-TS}} = 155 \pm 30$ cal/mol·K) (*SI Appendix*, Fig. S5). The value of ΔC_p is directly proportional to the change in the number of dof (Δn), $\Delta C_p = \Delta n \cdot k_B/2$, which gives $\Delta n \sim$1 per cal/K·mol unit in ΔC_p. This gives $\Delta n^{\text{TS-U}} \sim 900 \gg \Delta n^{\text{N-TS}} \sim 150$, showing that the main configurational entropy loss occurs upon forming the TS from U. This result depicts the TS as a molten globule of high free energy ($\Delta G^{\ddagger} \sim \Delta G_0$) and low configurational entropy ($\Delta C_p^{\text{N-TS}} \ll \Delta C_p$), which is structurally similar to the N: The major change in ΔC_p and Δn occurs between U and TS.

Discussion

We have used calorimetric optical tweezers to measure the FDCs of protein barnase in the range 7 °C to 37 °C and derived the folding thermodynamics at the single-molecule level. An analysis based on the Clausius–Clapeyron equation (Eq. **2**) was used to extract the temperature-dependent values of $\Delta S_0(T)$ and $\Delta H_0(T)$, and ΔC_p. These agree with those obtained from bulk experiments in our conditions of ionic strength (20 mM

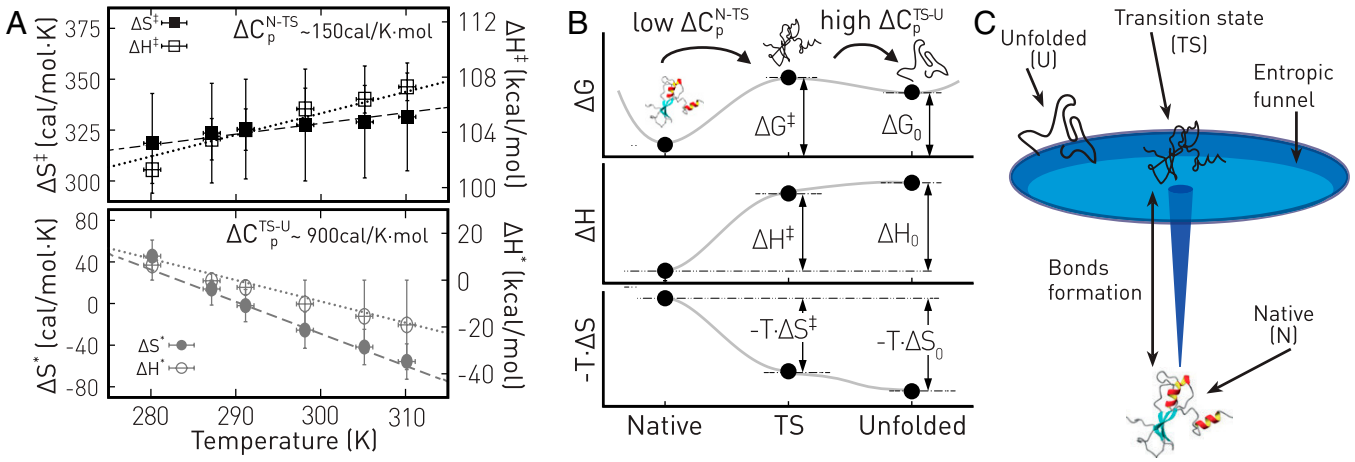

Fig. 6. Barnase free-energy landscape. (*A*) Entropy (full symbols) and enthalpy (empty symbols) differences between N and TS (‡, black); and between U and TS (*, gray). (*B*) Illustration of the free-energy (ΔG, *Top*), enthalpy (ΔH, *Middle*), and entropy ($-T \cdot \Delta S$, *Bottom*) landscape relative to N. (*C*) Golf course folding free-energy landscape of barnase highlighting the molten globule structure formed in the TS.

monovalent salt) and neutral pH (7.0). The mean values for the enthalpy, entropy, and T_m derived from the work-FT and kinetic analysis ($\Delta H_0^m = 140 \pm 2$ kcal/mol, $\Delta S_0^m = 434 \pm 10$ cal/mol·K, and $T_m = 50 \pm 2$ °C) agree with those reported in the literature and collected in ref. 65, $\Delta H_m \sim 115$ kcal/mol to 145 kcal/mol and $\Delta S_m \sim 400$ cal/mol·K (summarized in *SI Appendix*, Table S1). Our estimation of $\Delta C_p = 1050 \pm 50$ cal/mol·K also agrees with values obtained from differential scanning and isothermal titration calorimetry assays, $\Delta C_p \sim 1,450 \pm 250$ cal/mol·K (*SI Appendix*, Table S1), as well as with recent atomistic numerical simulations (66). Measurements of ΔC_p in calorimetric experiments often require determining the temperature dependence of ΔH with pH, ionic strength, or the denaturant concentration. In contrast, with CFS, we directly measure thermodynamic potentials and kinetics at a given temperature. In *SI Appendix*, Fig. S3, we also compare the protein stability curve of barnase derived from the fits to Eqs.**7a** and **7b** with that reported in calorimetric studies (67, 68) and numerical simulations (66).

Remarkably, entropies and enthalpies between the TS and the U (ΔS^*, ΔH^*, and ΔG^*), are ∼10 times lower than the corresponding ones between TS and the N ($\Delta S^\ddagger$, $\Delta H^\ddagger$, and $\Delta G^\ddagger$). In fact, the low value of ΔG^* correlates with the high compliance of the molten globule upon stretching, as has been shown for apomyoglobin (28). A general feature of free energies $(0, \ddagger, *)$ in Table 1 is the compensation observed between entropy ($T\Delta S$) and enthalpy (ΔH) contributions; that is, $\Delta G = \Delta H - T\Delta S \ll |\Delta H|, |T\Delta S|$. In contrast, the major contribution to ΔC_p occurs between U and TS ($\Delta C_p^{\mathrm{TS-U}} \gg \Delta C_p^{\mathrm{N-TS}}$). The value of $\Delta C_p^{\mathrm{TS-U}}$ is proportional to the reduction ($\Delta n^{\mathrm{TS-U}} \sim 900$) in the number of dof between TS and U, at a rate of ∼1 dof/(cal/K·mol).

Our results agree with the folding funnel scenario of the ELH (Fig. 6*C*), where a large configurational entropy loss (∼90%) occurs upon forming the TS from the U. Such entropy loss is accompanied by a low enthalpy change (∼20% of the total folding enthalpy). The large configurational entropy loss between U and TS demonstrates that folding is an entropically driven process in a golf course energy landscape, where the TS is the native hole. The collapse from TS to N forms most of the native bonds, accounting for most of the entropy and enthalpy of folding ($\Delta S_0 \simeq \Delta S^\ddagger, \Delta H_0 \simeq \Delta H^\ddagger$). Overall, our results also validate the main predictions of the ELH.

Are these results applicable to other proteins? Assuming an equal average enthalpy per native bond in N and TS, their structural similarity implies a low fraction of native bonds at TS, $f^\ddagger = \Delta H^*/\Delta H_0$. For barnase, $f^\ddagger \sim 0.2$ at T_m, a value that decreases as T is lowered being $f^\ddagger \sim 0$ at $T = 7$ °C. These results are at odds with the observation often made in computational studies that $f^\ddagger$ = 0.5 at the TS. Previous atomic force microscopy studies on the ddFLN4 protein domain in the range 5 °C to 37 °C show that $f^\ddagger$ increases with T, reaching a maximum ($f^\ddagger = 0.19$) at 37 °C (69). Apparently, the increase of TS stability with T facilitates the collapse from TS to N.

The TS of barnase features the properties of a dry molten globule: a native-like expanded structure with the backbone formed, but with side chains loosely packed (70). The dry molten globule has a large enthalpy relative to N ($\Delta H^\ddagger$) but a low $\Delta C_p^{\mathrm{N-TS}}$, the major contribution to ΔC_p being $\Delta C_p^{\mathrm{TS-U}}$, in agreement with our results. We hypothesize that folding proceeds in two steps. First (U to TS), hydrophobicity (71) drives the formation of the barnase backbone by the stabilization of the four α-helices and β-strands and the expulsion of water from the protein core. The small difference between the net number of H bonds between U and TS leads to small values of $\Delta H^*, \Delta S^*$ relative to $\Delta H_0, \Delta S_0$. Next (TS to N), the dry molten globule collapses to N, stabilized by the liquid-like Van der Waals interactions between the loosely packed side chains in TS. The $1/r^6$ dependence of Van der Waals interactions implies a large $\Delta H^\ddagger$ even for a short-distance collapse. $\Delta H^\ddagger$ is compensated by $T\Delta S^\ddagger$ (enthalpy–entropy compensation), a generic feature of weak interactions. Pushing the analogy further, protein folding resembles planet formation, where the mantle forms first and the core solidifies afterward.

Alternatively, in a wet molten globule, the backbone is formed at TS, but water remains inside the protein core. A wet molten globule would lead to a high free-energy barrier to folding, ΔG^*, and a two-state folding scenario. Instead, $\Delta G^* = 2 \pm 3$ kcal/mol at T_m and is negative below T_m (Table 1). Remarkably, our results support the downhill folding (rather than two states) scenario (72–74), correlating it with the MGH.

Our results do not exclude the FH picture, where proteins fold along a well-defined pathway by the sequential formation of foldons. In the FH, the free-energy landscape resembles the ELH golf course shown in Fig. 6*C*, except for the fact that it incorporates a specific folding pathway (groove) along the ground with one or more intermediates (*SI Appendix*, Fig. S6). Discriminating between the ELH and FH would require monitoring folding paths in configurational space. Bulk measurements have addressed this question by combining hydrogen exchange (75) and NMR (76). In single-molecule experiments, one might measure reaction coordinates other than the molecular extension, for example, in multiple-color fluorescence resonance energy transfer (77), atomistic simulations (78, 79), and changing environmental conditions and mutations (80). Reproducible patterns in the folding trajectories are evidence of a preferential folding pathway in the energy landscape, supporting the FH.

Summing up, CFS permits measuring folding entropies and enthalpies over a broad temperature range, with the accuracy necessary to determine heat capacity changes. In conjunction with a detailed kinetics study, this permits us to determine barrier entropies, enthalpies, and heat capacity changes relative to the N and U. Three thermodynamic inequalities summarize our results: $|\Delta S^*| \ll \Delta S^\ddagger, |\Delta H^*| \ll \Delta H^\ddagger$, and $\Delta C_p^{\mathrm{TS-U}} \gg \Delta C_p^{\mathrm{N-TS}}$. These are key inequalities for molecular folding in line with predictions of the molten globule and energy landscape hypotheses. In particular, accurate measurements of ΔC_p are crucial to quantify to what extent configurational entropy loss drives intermediates formation and folding. Our study might be extended to other proteins, RNAs, and ligand–substrate binding (64, 81, 82). In the latter, the ligand docks into the binding site of the substrate by searching in configurational space, similarly to finding the TS in protein folding. Docking is then followed by the assembly of the ligand–substrate complex, analogously to the TS–N collapse in protein folding.

Materials and Methods

Molecular Construct and Experimental Setup. For pulling experiments, barnase is expressed between two identical double-stranded DNA (dsDNA) (500 bp) handles, which are attached to the N and C termini via cysteine thiol chemical reduction (details in ref. 49). The 5′ end of one handle is labeled with a biotin, while the 3′ end of the other handle is labeled with a digoxigenin. The biotin- and digoxigenin-labeled ends specifically bind to streptavidin (SA) and antidigoxigenin (AD) coated beads. For the pulling experiments (Fig. 1*C*), one end is attached to the SA bead, which is kept fixed at the tip of a glass micropipette by air suction, whereas the other end is attached to the AD bead captured in

the optical trap. Force changes by varying the relative distance λ between the center of the optical trap and the bead in the pipette. In pulling experiments, the optical trap is moved up and down at a given speed and force ramped between an initial force ($\approx$1 pN to 2 pN), where the molecule is folded, and a maximum force ($\sim$30 pN), where barnase is unfolded. The unfolding transition is detected as a force rip in the force versus λ curve (FDC). Moreover, due to the folding reversibility of barnase, it refolds upon reducing λ and the force.

To perform CFS experiments, we used the temperature-jump optical trap described in ref. 42. Briefly, a collimated laser at 1,435-nm wavelength (heating laser) is used to heat uniformly a $\sim$100-μm-radius area in the center of the fluidics chamber where the experiments are carried out. The wavelength is chosen to maximize the absorption by the water in the buffer solution (10 mM of Na_2HPO_4 and NaH_2PO_4 at pH 7.0) to heat the surrounding medium to locally raise the temperature from 25 °C (room temperature) to 40 °C. Moreover, we can place the miniaturized optical tweezers instrument inside an icebox kept at 5 °C and heat from this basal temperature up to 25 °C using the heating laser. In this way, the available temperature ranges from 5 °C to 40 °C.

Folding Free Energy at Zero Force. To derive the folding free energy at zero force, ΔG_0, from force experiments, we consider four different states of the protein (Fig. 2*C*, circled numbers): state 1, folded barnase at zero force; state 2, folded barnase at a given force *f;* state 3, unfolded barnase at the same force *f;* and state 4, unfolded barnase at zero force. Notice that the direct unfolding pathway at zero force $1 \rightarrow 4$, observed in bulk experiments, can be decomposed as the sum of three sequential steps ($1 \rightarrow 4 = 1 \rightarrow 2 + 2 \rightarrow 3 + 3 \rightarrow 4$). The three steps are as follows. For step $1 \rightarrow 2$, folded barnase is reversibly pulled from zero force to force *f* along the native branch of the FDC (Fig. 2 *C*, *Left Inset*, black dashed line). The free-energy difference equals the sum of the reversible work to orient a dipole of length equal to the distance between the N and C termini of folded barnase [$\simeq$ 3 nm (49)], $\Delta G_{\rm d}(0 \rightarrow f)$, and the reversible work of stretching the handles and displacing the bead in the optical trap, $\Delta G_{\rm h\text{-}b}(0 \rightarrow f)$. For step $2 \rightarrow 3$, folded barnase is reversibly unfolded (denatured) at a constant force *f*. In this step, the free-energy difference, $\Delta G(f)$, equals the free energy of the stretched polypeptide chain minus the folding free energy of native barnase, at force *f*. For step $3 \rightarrow 4$, the stretched polypeptide chain is reversibly relaxed from *f* to zero force along the unfolded branch of the FDC (Fig. 2 *C*, *Left Inset*, gray solid line). The free-energy difference equals the reversible work of releasing the polypeptide chain from force *f* to 0 ($-\Delta G_{\rm p}(0 \rightarrow f)$) plus the reversible work of relaxing the handles and the bead in the optical trap from *f* to zero (equal to $-\Delta G_{\rm h\text{-}b}(0 \rightarrow f)$, from step $1 \rightarrow 2$). Thermodynamic energy differences are path independent, so $\Delta G(1 \rightarrow 4) = \Delta G(1 \rightarrow 2) + \Delta G(2 \rightarrow 3) + \Delta G(3 \rightarrow 4)$. This gives

$$\Delta G_0 = \Delta G_{\rm d}(0 \rightarrow f) + \Delta G(f) - \Delta G_{\rm p}(0 \rightarrow f). \qquad \textbf{[12]}$$

The same balance equation holds for ΔH_0, ΔS_0, and ΔC_p. Notice that $\Delta G_{\rm h\text{-}b}(0 \rightarrow f)$ does not appear in Eq. **12**, as it cancels out when adding steps $1 \rightarrow 2$ and $3 \rightarrow 4$ (see *SI Appendix*, section S1 for details).

The unfolding transition at constant force can be measured in instruments where the intensive variable, that is, the force, is the natural control parameter (e.g., in magnetic tweezers). In contrast, in optical tweezers, force cannot be controlled unless force feedback is applied (43). As a consequence, the unfolding transition does not occur at fixed force *f* but at fixed λ. Indeed, when pulling with optical tweezers, the unfolding transition is observed as a force rip in the FDC (dark arrows in Fig. 2*B*) which occurs at fixed λ. Therefore, free-energy differences in the force ensemble, $\Delta G(f)$, are Legendre transforms of those measured in the λ-ensemble (83).

A major contribution in Eq. **12** is the elastic term $\Delta G_{\rm p}$ for the polypeptide chain, which is often modeled as a semiflexible polymer. The term $\Delta G_{\rm d}$ stands for the elastic energy of aligning a molecular-sized dipole along the force axis. As the dipole extension is much shorter than the contour length of the polypeptide chain, $\Delta G_{\rm p}(0 \rightarrow f) \gg \Delta G_{\rm d}(0 \rightarrow f)$ at all forces. The relative magnitude of $\Delta G_{\rm p}(0 \rightarrow f)$ and $\Delta G(f)$ depends on the difference between *f* and the coexistence force f_c, which is defined as the force at which the folded and unfolded barnases have equal free energies; that is, $\Delta G(f_c) = 0$. Eq. **12** gives, for $f = f_c$,

$$\Delta G_0 = -\Delta G_{\rm p}(0 \rightarrow f_c) + \Delta G_{\rm d}(0 \rightarrow f_c)\,. \qquad \textbf{[13]}$$

The stretching free energy of the different elastic elements at a given force *f* can be obtained by using the well-known expression (83)

$$\Delta G_{\rm i}(0 \rightarrow f) = -\int_0^f x_{\rm i}(f')df', \qquad \textbf{[14]}$$

where $\rm i \equiv p,d$, whereas the difference in the trap position $\Delta\lambda$ between the unfolded and native branches at a given force *f* (Fig. 2 *B*, *Right Inset*) equals

$$\Delta\lambda(f) = x_{\rm p}(f) - -x_{\rm d}(f)\ . \qquad \textbf{[15]}$$

Combining the previous equations, we obtain the relation

$$\Delta G_0(T) = \int_0^{f_c(T)} \Delta\lambda(f,T)df\,, \qquad \textbf{[16]}$$

showing that the knowledge of $f_c(T)$ and the measured $\Delta\lambda(f,T)$ permits determination of ΔG_0 at a given temperature *T*. Eq. **16** is the basic thermodynamic formula we will use to determine $\Delta S_0(T)$, $\Delta H_0(T)$, and ΔC_p in barnase folding.

Data Availability. All study data are included in the article and/or *SI Appendix*.

ACKNOWLEDGMENTS. M.R.-P. and F.R. acknowledge financial support from Grants Proseqo (FP7 EU program) FIS2016-80458-P (Spanish Research Council), Icrea Academia prizes 2013 and 2018 (Catalan government), and Spanish Research Council Grant PID2019-111148GB-I00. A.Z. acknowledges funding from Padua University Supply Award 2015 6710927028 and Fondazione Cariparo Visiting Programme 2018 (project "Time-resolved Force Spectroscopy of Single DNA molecules").

Author affiliations: [a]Small Biosystems Lab, Condensed Matter Physics Department, University of Barcelona, 08028 Barcelona, Spain; [b]Physics and Astronomy Department, University of Padova, 35131 Padova, Italy; [c]Laboratory of Nanoscale Biology, Institute of Bioengineering, School of Engineering, Ecole Polytechnique Federale de Lausanne, 1015 Lausanne, Switzerland; and [d]SpliceBio, 08028 Barcelona, Spain

1. C. B. Anfinsen, E. Haber, M. Sela, F. H. White Jr., The kinetics of formation of native ribonuclease during oxidation of the reduced polypeptide chain. *Proc. Natl. Acad. Sci. U.S.A.* **47**, 1309–1314 (1961).
2. C. B. Anfinsen, Principles that govern the folding of protein chains. *Science* **181**, 223–230 (1973).
3. C. Levinthal, Are there pathways for protein folding? *J. Chim. Phys.* **65**, 44–45 (1968).
4. K. A. Dill, Dominant forces in protein folding. *Biochemistry* **29**, 7133–7155 (1990).
5. O. B. Ptitsyn, Molten globule and protein folding. *Adv. Protein Chem.* **47**, 83–229 (1995).
6. L. Hua, R. Zhou, D. Thirumalai, B. J. Berne, Urea denaturation by stronger dispersion interactions with proteins than water implies a 2-stage unfolding. *Proc. Natl. Acad. Sci. U.S.A.* **105**, 16928–16933 (2008).
7. S. K. Jha, S. Marqusee, Kinetic evidence for a two-stage mechanism of protein denaturation by guanidinium chloride. *Proc. Natl. Acad. Sci. U.S.A.* **111**, 4856–4861 (2014).
8. A. Matouschek, J. T. Kellis Jr., L. Serrano, A. R. Fersht, Mapping the transition state and pathway of protein folding by protein engineering. *Nature* **340**, 122–126 (1989).
9. R. L. Baldwin, G. D. Rose, Molten globules, entropy-driven conformational change and protein folding. *Curr. Opin. Struct. Biol.* **23**, 4–10 (2013).
10. M. Dijkstra, W. Fokkink, J. Heringa, E. van Dijk, S. Abeln, The characteristics of molten globule states and folding pathways strongly depend on the sequence of a protein. *Mol. Phys.* **116**, 3173–3180 (2018).
11. H. Frauenfelder, S. G. Sligar, P. G. Wolynes, The energy landscapes and motions of proteins. *Science* **254**, 1598–1603 (1991).
12. J. D. Bryngelson, J. N. Onuchic, N. D. Socci, P. G. Wolynes, Funnels, pathways, and the energy landscape of protein folding: A synthesis. *Proteins* **21**, 167–195 (1995).
13. R. L. Baldwin, The nature of protein folding pathways: The classical versus the new view. *J. Biomol. NMR* **5**, 103–109 (1995).
14. H. Maity, M. Maity, M. M. Krishna, L. Mayne, S. W. Englander, Protein folding: The stepwise assembly of foldon units. *Proc. Natl. Acad. Sci. U.S.A.* **102**, 4741–4746 (2005).
15. C. J. Camacho, D. Thirumalai, Kinetics and thermodynamics of folding in model proteins. *Proc. Natl. Acad. Sci. U.S.A.* **90**, 6369–6372 (1993).
16. K. A. Dill, J. L. MacCallum, The protein-folding problem, 50 years on. *Science* **338**, 1042–1046 (2012).
17. A. Borgia, P. M. Williams, J. Clarke, Single-molecule studies of protein folding. *Annu. Rev. Biochem.* **77**, 101–125 (2008).
18. D. Thirumalai, E. P. O'Brien, G. Morrison, C. Hyeon, Theoretical perspectives on protein folding. *Annu. Rev. Biophys.* **39**, 159–183 (2010).
19. C. Bustamante, L. Alexander, K. Maciuba, C. M. Kaiser, Single-molecule studies of protein folding with optical tweezers. *Annu. Rev. Biochem.* **89**, 443–470 (2020).

20. P. Cossio, G. Hummer, A. Szabo, Transition paths in single-molecule force spectroscopy. *J. Chem. Phys.* **148**, 123309 (2018).
21. C. M. Kaiser, D. H. Goldman, J. D. Chodera, I. Tinoco Jr., C. Bustamante, The ribosome modulates nascent protein folding. *Science* **334**, 1723–1727 (2011).
22. E. Infante *et al.*, The mechanical stability of proteins regulates their translocation rate into the cell nucleus. *Nat. Phys.* **15**, 973–981 (2019).
23. C. Cecconi, E. A. Shank, C. Bustamante, S. Marqusee, Direct observation of the three-state folding of a single protein molecule. *Science* **309**, 2057–2060 (2005).
24. F. Stockmar, A. Y. Kobitski, G. U. Nienhaus, Fast folding dynamics of an intermediate state in RNase H measured by single-molecule FRET. *J. Phys. Chem. B* **120**, 641–649 (2016).
25. J. C. M. Gebhardt, T. Bornschlögl, M. Rief, Full distance-resolved folding energy landscape of one single protein molecule. *Proc. Natl. Acad. Sci. U.S.A.* **107**, 2013–2018 (2010).
26. K. Neupane, A. P. Manuel, M. T. Woodside, Protein folding trajectories can be described quantitatively by one-dimensional diffusion over measured energy landscapes. *Nat. Phys.* **12**, 700–703 (2016).
27. J. Stigler, F. Ziegler, A. Gieseke, J. C. M. Gebhardt, M. Rief, The complex folding network of single calmodulin molecules. *Science* **334**, 512–516 (2011).
28. P. J. Elms, J. D. Chodera, C. Bustamante, S. Marqusee, The molten globule state is unusually deformable under mechanical force. *Proc. Natl. Acad. Sci. U.S.A.* **109**, 3796–3801 (2012).
29. S. Lindhoud, M. Pirchi, A. H. Westphal, G. Haran, C. P. van Mierlo, Gradual folding of an off-pathway molten globule detected at the single-molecule level. *J. Mol. Biol.* **427**, 3148–3157 (2015).
30. T. R. Sosnick, L. Mayne, R. Hiller, S. W. Englander, The barriers in protein folding. *Nat. Struct. Biol.* **1**, 149–156 (1994).
31. A. R. Fersht, Characterizing transition states in protein folding: An essential step in the puzzle. *Curr. Opin. Struct. Biol.* **5**, 79–84 (1995).
32. A. Tikhomirova, N. Taulier, T. V. Chalikian, Energetics of nucleic acid stability: The effect of DeltaCP. *J. Am. Chem. Soc.* **126,** 16387–16394 (¿2004).
33. C. M. Johnson, Differential scanning calorimetry as a tool for protein folding and stability. *Arch. Biochem. Biophys.* **531**, 100–109 (2013).
34. J. K. Myers, C. N. Pace, J. M. Scholtz, Denaturant m values and heat capacity changes: Relation to changes in accessible surface areas of protein unfolding. *Protein Sci.* **4**, 2138–2148 (1995).
35. J. Gómez, V. J. Hilser, D. Xie, E. Freire, The heat capacity of proteins. *Proteins* **22**, 404–412 (1995).
36. S. B. Smith, Y. Cui, C. Bustamante, Optical-trap force transducer that operates by direct measurement of light momentum. *Methods Enzymol.* **361**, 134–162 (2003).
37. I. Tinoco Jr., C. Bustamante, The effect of force on thermodynamics and kinetics of single molecule reactions. *Biophys. Chem.* **101-102**, 513–533 (2002).
38. D. Keller, D. Swigon, C. Bustamante, Relating single-molecule measurements to thermodynamics. *Biophys. J.* **84**, 733–738 (2003).
39. F. Ritort, Single-molecule experiments in biological physics: Methods and applications. *J. Phys. Condens. Matter* **18**, R531–R583 (2006).
40. M. C. Williams, J. R. Wenner, I. Rouzina, V. A. Bloomfield, Entropy and heat capacity of DNA melting from temperature dependence of single molecule stretching. *Biophys. J.* **80**, 1932–1939 (2001).
41. W. Stephenson *et al.*, Combining temperature and force to study folding of an RNA hairpin. *Phys. Chem. Chem. Phys.* **16**, 906–917 (2014).
42. S. de Lorenzo, M. Ribezzi-Crivellari, J. R. Arias-Gonzalez, S. B. Smith, F. Ritort, A temperature-jump optical trap for single-molecule manipulation. *Biophys. J.* **108**, 2854–2864 (2015).
43. M. Rico-Pasto, I. Pastor, F. Ritort, Force feedback effects on single molecule hopping and pulling experiments. *J. Chem. Phys.* **148**, 123327 (2018).
44. C. Martin, V. Richard, M. Salem, R. Hartley, Y. Mauguen, Refinement and structural analysis of barnase at 1.5 Å resolution. *Acta Crystallogr. D Biol. Crystallogr.* **55**, 386–398 (1999).
45. V. A. Mitkevich *et al.*, Thermodynamics of denaturation of complexes of barnase and binase with barstar. *Biophys. Chem.* **105**, 383–390 (2003).
46. M. Bycroft, A. Matouschek, J. T. Kellis Jr., L. Serrano, A. R. Fersht, Detection and characterization of a folding intermediate in barnase by NMR. *Nature* **346**, 488–490 (1990).
47. R. B. Best, B. Li, A. Steward, V. Daggett, J. Clarke, Can non-mechanical proteins withstand force? Stretching barnase by atomic force microscopy and molecular dynamics simulation. *Biophys. J.* **81**, 2344–2356 (2001).
48. X. Salvatella, C. M. Dobson, A. R. Fersht, M. Vendruscolo, Determination of the folding transition states of barnase by using ϕi-value-restrained simulations validated by double mutant ϕij-values. *Proc. Natl. Acad. Sci. U.S.A.* **102**, 12389–12394 (2005).
49. A. Alemany, B. Rey-Serra, S. Frutos, C. Cecconi, F. Ritort, Mechanical folding and unfolding of protein barnase at the single-molecule level. *Biophys. J.* **110**, 63–74 (2016).
50. A. Severino, A. M. Monge, P. Rissone, F. Ritort, Efficient methods for determining folding free energies in single-molecule pulling experiments. *J. Stat. Mech. Theory Exp.* **2019**, 124001 (2019).
51. C. Bustamante, J. F. Marko, E. D. Siggia, S. Smith, Entropic elasticity of lambda-phage DNA. *Science* **265**, 1599–1600 (1994).
52. C. Bouchiat *et al.*, Estimating the persistence length of a worm-like chain molecule from force-extension measurements. *Biophys. J.* **76**, 409–413 (1999).
53. D. Collin *et al.*, Verification of the Crooks fluctuation theorem and recovery of RNA folding free energies. *Nature* **437**, 231–234 (2005).
54. C. Jarzynski, Equalities and inequalities: Irreversibility and the second law of thermodynamics at the nanoscale. *Annu. Rev. Condens. Matter Phys.* **2**, 329–351 (2011).
55. M. Palassini, F. Ritort, Improving free-energy estimates from unidirectional work measurements: Theory and experiment. *Phys. Rev. Lett.* **107**, 060601 (2011).
56. M. R. Shirts, E. Bair, G. Hooker, V. S. Pande, Equilibrium free energies from nonequilibrium measurements using maximum-likelihood methods. *Phys. Rev. Lett.* **91**, 140601 (2003).
57. N. Forns *et al.*, Improving signal/noise resolution in single-molecule experiments using molecular constructs with short handles. *Biophys. J.* **100**, 1765–1774 (2011).
58. S. Geggier, A. Kotlyar, A. Vologodskii, Temperature dependence of DNA persistence length. *Nucleic Acids Res.* **39**, 1419–1426 (2011).
59. D. K. Klimov, D. Thirumalai, Stretching single-domain proteins: Phase diagram and kinetics of force-induced unfolding. *Proc. Natl. Acad. Sci. U.S.A.* **96**, 6166–6170 (1999).
60. C. Hyeon, D. Thirumalai, Mechanical unfolding of RNA hairpins. *Proc. Natl. Acad. Sci. U.S.A.* **102**, 6789–6794 (2005).
61. A. Imparato, A. Pelizzola, M. Zamparo, Equilibrium properties and force-driven unfolding pathways of RNA molecules. *Phys. Rev. Lett.* **103**, 188102 (2009).
62. C. Hyeon, D. Thirumalai, Measuring the energy landscape roughness and the transition state location of biomolecules using single molecule mechanical unfolding experiments. *J. Phys. Condens. Matter* **19**, 113101 (2007).
63. M. Rico-Pasto, A. Zaltron, F. Ritort, Force dependence of proteins' transition state position and the Bell–Evans model. *Nanomaterials (Basel)* **11**, 3023 (2021).
64. L. Rognoni, J. Stigler, B. Pelz, J. Ylänne, M. Rief, Dynamic force sensing of filamin revealed in single-molecule experiments. *Proc. Natl. Acad. Sci. U.S.A.* **109**, 19679–19684 (2012).
65. W. Pfeil, *Protein Stability and Folding Supplement 1: A Collection of Thermodynamic Data* (Springer Science & Business Media, 2012).
66. J. J. Galano-Frutos, J. Sancho, Accurate calculation of barnase and snase folding energetics using short molecular dynamics simulations and an atomistic model of the unfolded ensemble: Evaluation of force fields and water models. *J. Chem. Inf. Model.* **59**, 4350–4360 (2019).
67. Y. V. Griko, G. I. Makhatadze, P. L. Privalov, R. W. Hartley, Thermodynamics of barnase unfolding. *Protein Sci.* **3**, 669–676 (1994).
68. A. A. Makarov *et al.*, Comparative study of thermostability and structure of close homologues–Barnase and binase. *J. Biomol. Struct. Dyn.* **10**, 1047–1065 (1993).
69. M. Schlierf, M. Rief, Temperature softening of a protein in single-molecule experiments. *J. Mol. Biol.* **354**, 497–503 (2005).
70. R. L. Baldwin, C. Frieden, G. D. Rose, Dry molten globule intermediates and the mechanism of protein unfolding. *Proteins* **78**, 2725–2737 (2010).
71. T. Imai, Y. Harano, M. Kinoshita, A. Kovalenko, F. Hirata, Theoretical analysis on changes in thermodynamic quantities upon protein folding: Essential role of hydration. *J. Chem. Phys.* **126**, 06B606 (2007).
72. W. A. Eaton, Searching for "downhill scenarios" in protein folding. *Proc. Natl. Acad. Sci. U.S.A.* **96**, 5897–5899 (1999).
73. V. Muñoz, J. M. Sanchez-Ruiz, Exploring protein-folding ensembles: A variable-barrier model for the analysis of equilibrium unfolding experiments. *Proc. Natl. Acad. Sci. U.S.A.* **101**, 17646–17651 (2004).
74. J. Liu *et al.*, Exploring one-state downhill protein folding in single molecules. *Proc. Natl. Acad. Sci. U.S.A.* **109**, 179–184 (2012).
75. S. W. Englander, L. Mayne, The case for defined protein folding pathways. *Proc. Natl. Acad. Sci. U.S.A.* **114**, 8253–8258 (2017).
76. M. Sadqi, D. Fushman, V. Muñoz, Atom-by-atom analysis of global downhill protein folding. *Nature* **442**, 317–321 (2006).
77. B. Schuler, E. A. Lipman, W. A. Eaton, Probing the free-energy surface for protein folding with single-molecule fluorescence spectroscopy. *Nature* **419**, 743–747 (2002).
78. K. Lindorff-Larsen, S. Piana, R. O. Dror, D. E. Shaw, How fast-folding proteins fold. *Science* **334**, 517–520 (2011).
79. J. Y. Kim, H. S. Chung, Disordered proteins follow diverse transition paths as they fold and bind to a partner. *Science* **368**, 1253–1257 (2020).
80. E. J. Guinn, B. Jagannathan, S. Marqusee, Single-molecule chemo-mechanical unfolding reveals multiple transition state barriers in a small single-domain protein. *Nat. Commun.* **6**, 6861 (2015).
81. M. M. Naqvi *et al.*, Single-molecule folding mechanisms of the apo- and Mg^{2+}-bound states of human neuronal calcium sensor-1. *Biophys. J.* **109**, 113–123 (2015).
82. P. Sonar *et al.*, Effects of ligand binding on the energy landscape of acyl-CoA-binding protein. *Biophys. J.* **119**, 1821–1832 (2020).
83. A. M. Monge, M. Manosas, F. Ritort, Experimental test of ensemble inequivalence and the fluctuation theorem in the force ensemble in DNA pulling experiments. *Phys. Rev. E* **98**, 032146 (2018).